*energies*

MDPI

*Article*

# Full-Bridge T-Type Three-Level LLC Resonant Converter with Wide Output Voltage Range

**Kangjia Zhang [1], Kun Zhao [1], Xiaoxiao Yang [1], Muyang Liu [1] and Zhigang Yao [2,*]**

[1] National Rail Transit Electrification and Automation Engineering Technology Research Center, Southwest Jiao Tong University, Chengdu 611756, China; zkj0825@my.swjtu.edu.cn (K.Z.); zhaokun@my.swjtu.edu.cn (K.Z.); xiaoxyang@my.swjtu.edu.cn (X.Y.); 2021200442@my.swjtu.edu.cn (M.L.)
[2] Energy Research Institute, Nanyang Technological University, Singapore 639798, Singapore
* Correspondence: zhigang.yao@ntu.edu.sg; Tel.: +86-13368363187

**Abstract**

Traditional LLC resonant converters face significant challenges in wide-output-voltage-applications, such as limited voltage gain, efficiency degradation under wide-gain range, and increased complexity in magnetic component design. For example, in electric vehicle charging power modules, achieving wide output voltage typically relies on changing the transformer turns ratio or switching the series-parallel circuit configuration via relays, which prevents real-time dynamic adjustment. To overcome these limitations, this paper proposes a wide-gain-range control method based on a full-bridge T-type three-level LLC resonant converter, capable of achieving a voltage gain range exceeding six times. By integrating a T-type three-level bridge arm with PWM modulation and employing a variable-topology and variable-frequency control strategy, the proposed method achieves synergistic optimization for wide-output-voltage-applications. PWM modulation enables wide-range voltage output by dynamically adjusting both the converter topology and switching frequency. Finally, the proposed method is validated through circuit simulations and experimental results based on a full-bridge T-type three-level LLC converter prototype, demonstrating its effectiveness and feasibility.

**Keywords:** LLC resonant converter; T-type three-level; wide gain range

check for updates

Academic Editor: Hervé Morel

Received: 27 July 2025
Revised: 26 August 2025
Accepted: 27 August 2025
Published: 30 August 2025

**Citation:** Zhang, K.; Zhao, K.; Yang, X.; Liu, M.; Yao, Z. Full-Bridge T-Type Three-Level LLC Resonant Converter with Wide Output Voltage Range. *Energies* **2025**, *18*, 4613. https://doi.org/10.3390/en18174613

**Copyright:** © 2025 by the authors. Licensee MDPI, Basel, Switzerland. This article is an open access article distributed under the terms and conditions of the Creative Commons Attribution (CC BY) license (https://creativecommons.org/licenses/by/4.0/).

## 1. Introduction

As a highly efficient power conversion scheme, the LLC resonant converter is widely used in various types of power electronic devices, particularly in medium- and high-power applications that require high efficiency, low loss, and low electromagnetic interference (EMI). Its most significant advantage lies in the implementation of soft-switching operation, which enables the converter to maintain zero-voltage-switching (ZVS) or zero-current-switching (ZCS) states during both conduction and turn-off of the switching devices. This capability effectively reduces switching losses and electromagnetic interference [1–3]. The soft-switching feature allows the LLC resonant converter to maintain high efficiency even at high frequencies, making it especially suitable for high-frequency, high-power-density applications such as high-efficiency power supplies and electric vehicle charging systems [4,5].

However, the frequency regulation range of LLC resonant converters is typically narrow. When operating far from the resonant frequency, conventional adjustments to the duty cycle or phase shift angle may fail to maintain soft-switching, leading to increased

switching currents in the power devices and a significant drop in efficiency [6,7]. This limitation poses challenges for achieving wide output voltage ranges, especially under large load variations, where system efficiency can degrade substantially [8].

Many existing wide gain control methods primarily rely on adjusting the gain near the resonance point [9,10], but this approach limits the converter's output voltage range to some extent. To address this issue, researchers have proposed various topology design schemes, with full-bridge LLC and half-bridge LLC being the most common structures. These topologies achieve a wider output voltage range within a certain range by adjusting the frequency, duty cycle, and phase shift angle [11–15]. However, they still have a limited gain range and pose significant design challenges under efficient operating conditions [16,17].

To address this issue, multilevel topologies have gained increasing attention in recent years. By increasing the number of levels, multilevel topologies can significantly reduce the voltage stress on the switching devices and provide a stable output across a wider voltage range [18–20]. For instance, converters with three or more levels can not only extend the gain range but also enhance both the efficiency and power density of the system [21–23]. However, the adoption of multilevel topologies often comes with more complex control strategies and higher cost burdens, particularly in high-power applications [24,25]. Additionally, adjusting the transformer turns ratio is a common method to extend the gain range. By altering the turns ratio or modifying the topology, the voltage gain can be adjusted within a specific range, thus enabling a wider output voltage [26–30]. However, this approach is constrained by factors such as transformer size, cost, and magnetic materials, making it unsuitable for all application scenarios [31].

Another three-level topology is the T-type three-level LLC converter. This topology typically includes four switching tubes, though only three are required when the T-type bridge is replaced by a bidirectional switch, which helps achieve low conduction losses and reduced switching stress [32]. The T-type bridge has also evolved into a hybrid bridge topology, which meets the wide gain requirement through frequency shifting [33]. Furthermore, recent research on the T-type three-level LLC converter has focused on widening the gain range of the T-type bridge LLC converter by achieving a 0.25-fold gain through alternating modulation of the topology [34–36]. Reference [34] indicates that the T-type bridge structure exhibits lower on-resistance and voltage drop compared to stacked half-bridge and NPC three-level LLC converters [37,38]. As illustrated in Figure 1, the switch network of the T-type bridge demonstrates reduced conduction resistance and voltage drop. Specifically, for power semiconductor devices with the same current rating and technology generation, the conduction resistance of a 1200 V SiC MOSFET is lower than the combined resistance of two 650 V SiC MOSFETs connected in series. Likewise, the conduction voltage drop of a 1200 V IGBT is less than that of two 650 V IGBTs in series. These characteristics indicate that the T-type three-level LLC converter achieves lower conduction losses, thereby improving overall system efficiency [39–41]. Reference [42] indicate that compared with T-type LLC resonant converters, dual-resonant cavity structures are more prone to current imbalance. In addition, the use of multiple transformers further increases the complexity of design and debugging. Additionally, the T-type three-level LLC converter is more cost-effective when using three independent drive supplies. The T-type bridge can also be replaced with bidirectional switches, further reducing the overall cost.

To expand the gain of the LLC converter while utilizing the advantages of the T-type bridge, this paper proposed a wide-range control method based on a full-bridge T-type three-level LLC resonant converter. The T-type three-level bridge arm reduces the voltage stress on the switching devices and extends the voltage gain range through multilevel modulation. Meanwhile, the wide-output-voltage design, which incorporates variable-

frequency and variable-topology control strategies, ensures soft-switching characteristics across the entire load range.

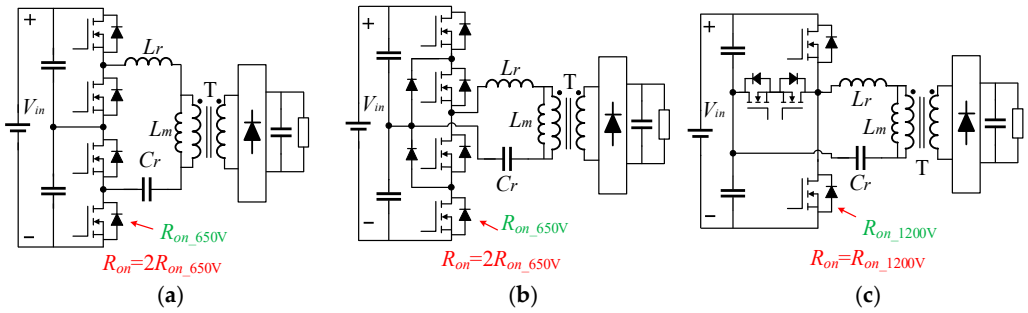



**Figure 1.** Conduction resistances at 0.5× normalized gain for common three-level topologies, with Vin = 800 V as an example. (**a**) Stacked half-bridge LLC converter; (**b**) NPC three-level LLC converter; (**c**) T-type three-level LLC converter.

The main contributions of this paper are as follows:

(1) This paper proposes a wide-range control method based on a full-bridge T-type three-level LLC resonant converter and analyzes the working principle and wide output voltage characteristic.
(2) A variable-topology strategy is employed to tackle the challenge of achieving both a wide output voltage range.
(3) A PWM modulation method is proposed to achieve a wide output voltage range through variable-topology and variable-frequency control strategies.

The structure of this paper is as follows: Section 2 describes in detail the conventional control methods to realize wide output voltage and their defects and shortcomings; Section 3 presents the variable-topology control strategy; Section 4 presents experimental results and comparative analyses; and Section 5 concludes the paper.

## 2. Conventional Control Method for Full-Bridge T-Type Three-Level LLC Resonant Converter

### *2.1. Operating Principle of the Full-Bridge T-Type Three-Level LLC Converter*

As shown in Figure 2, the topology full-bridge T-type LLC resonant converter utilizes two interleaved half-bridge T-type three-level converters operating with a 180° phase shift between phases. Each phase contains four power switches ($S_{a1}$–$S_{a4}$), where $S_{a1}$/$S_{a3}$ and $S_{a2}$/$S_{a4}$ operate as complementary pairs with a 50% duty cycle. The voltage divider capacitors ($C_{dc1}$, $C_{dc2}$) ensure balanced voltage distribution ($Vc_{dc1}$ = $Vc_{dc2}$), while the LLC resonant tank—comprising the resonant inductor ($L_r$), resonant capacitor ($C_r$), and the transformer's magnetizing inductance ($L_m$)—supports soft-switching operation. The secondary-side full-bridge rectifier ($D_1$–$D_4$), along with the output capacitor ($C_o$), provides a regulated DC output.

### *2.2. Analysis of Conventional Control Methods*

Conventional control methods often achieve a wide voltage output range by varying the duty cycle at frequencies higher than the resonant frequency. For example, Figure 3 shows the modulated waveform of a wide voltage output achieved by varying the duty cycle at frequencies greater than the resonant frequency.

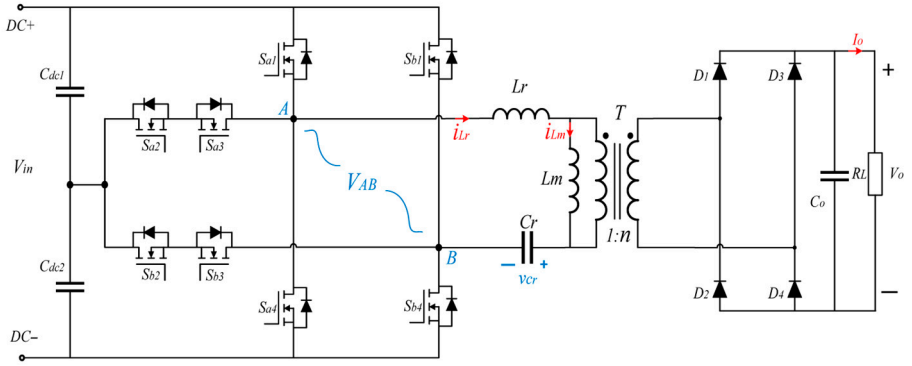



**Figure 2.** Topology of full-bridge T-type three-level LLC resonant converter.

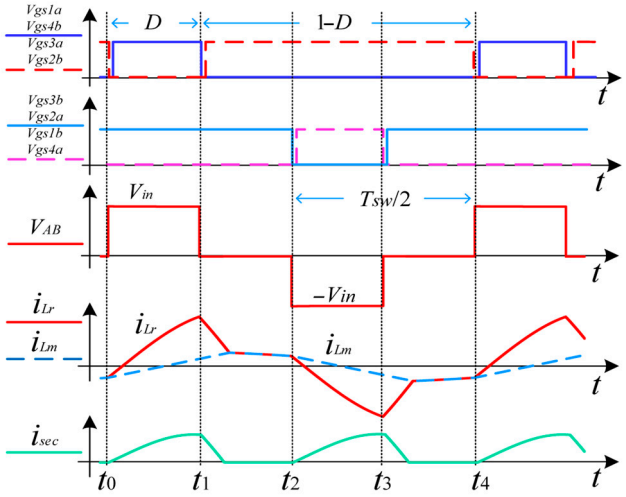



**Figure 3.** Waveform using variable duty cycle modulation when the switching frequency is less than the resonant frequency.

Phase [$t_0$–$t_1$]: During this phase, $S_{a1}$ and $S_{a2}$ of phase A conduct, while $S_{b3}$ and $S_{b4}$ of phase B conduct. The input voltage to the resonant cavity is equal to the input voltage of the system, and the resonant current is greater than the magnetizing current. The magnetizing inductance is clamped by the output voltage, causing the magnetizing current to rise linearly.

Phase [$t_1$–$t_2$]: At time $t_1$, $S_{a1}$ and $S_{b4}$ turn off. At this moment, the resonant current is greater than zero and is sustained by the body diodes of $S_{a3}$ and $S_{b2}$ (i.e., $S_{a2}$ and $S_{b3}$). The input voltage to the resonant cavity becomes zero, allowing for ZVS when $S_{a3}$ and $S_{b2}$ turn on. Once $S_{a3}$ and $S_{b2}$ are on, the resonant current decreases, while the magnetizing current continues to rise linearly. When the magnetizing current equals the resonant current, the magnetizing inductance and resonant capacitance jointly resonate with the resonant inductor and capacitor. At this point, the primary side of the transformer is decoupled from the secondary side, and the magnetizing inductance resonates with the resonant capacitor and resonant inductor.

Phase [$t_2$–$t_4$]: The converter enters the next half-cycle. When the voltages across $C_{dc1}$ and $C_{dc2}$ are equal, the waveform of the converter in the [$t_2$–$t_4$] phase becomes symmetrical to that of the [$t_0$–$t_2$] phase.

A wide voltage output range is often achieved by varying the switching frequency below the resonant frequency, as shown in Figure 4, which illustrates the modulation waveform at frequencies below the resonant frequency.

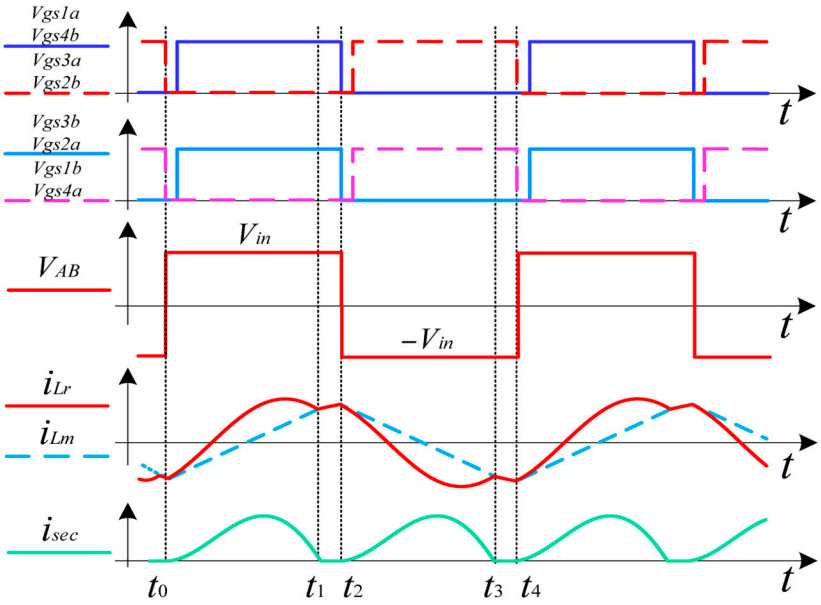



**Figure 4.** Waveform using variable frequency modulation when the switching frequency is less than the resonant frequency.

Phase [$t_0$–$t_1$]: At time $t_0$, the switching tubes $S_{a3}$ and $S_{b1}$ are turned off. Since the excitation inductance $L_m$ is relatively large and the duration of this mode is short, it can be approximated that the resonant inductance current remains unchanged. At this point, the resonance and excitation currents are equal. When the body diodes of $S_{a1}$ and $S_{b4}$ conduct, these transistors can be turned on at zero voltage. To ensure the zero-voltage turn-on of $S_{a1}$ and $S_{b4}$, they must be switched on before the current $i_{Lr}$ changes from negative to positive. As the source-drain voltages of $S_{a1}$ and $S_{b4}$ drop to zero, zero-voltage turn-on is achieved. At this point, the voltage between points A and B is $V_{in}$, and the rectifier diode $D_1$ conducts. The excitation inductance is then clamped at $V_o/n$, ceasing to participate in the resonance, while the excitation inductance current increases linearly. Meanwhile, the resonant network consisting of $L_r$ and $C_r$ begins to resonate, with the voltage across it being $V_{in} - V_o/n$.

Phase [$t_1$–$t_2$]: At time $t_1$, the current in the resonant inductor equals the excitation inductor current. At this moment, the current on the transformer secondary side is zero, effectively disconnecting the load from the resonant network. The rectifier diode $D_1$ is turned off, ensuring ZCS without any reverse recovery issues. The voltage across the excitation inductor $L_m$ is no longer clamped at $V_o/n$, and the resonant components $L_r$, $L_m$, and $C_r$ continue to resonate and operate.

Phase [$t_2$–$t_4$]: During this phase, the operating principle of the converter is similar to the second half of the previous operating cycle, so it will not be repeated here.

When the full-bridge T-type three-level LLC resonant converter operates at $f_s > f_r$, a wide voltage output range is achieved by varying the duty cycle. Additionally, when operating below the resonant frequency, a wide voltage output range is typically achieved using Pulse Frequency Modulation (PFM) converter control. The voltage gain function of the converter can be derived through fundamental approximation equivalent analysis:

$$G = \frac{\sin D\pi}{\sqrt{\left(1 + \frac{1}{k}\left(1 - \frac{1}{fn^2}\right)\right)^2 + \left(Q^2\left(fn - \frac{1}{fn}\right)^2\right)}} \quad (1)$$

where $k = L_m/L_r$, $f_n = f_s/f_r$, $f_s$ is the switching frequency, the resonant frequency is $fr = 1/2\pi\sqrt{L_rC_r}$, the quality factor is $Q = \sqrt{L_rC_r}/R_{eq}$, and $n$ is the transformer transformation ratio.

As shown in Figure 5, the traditional method achieves a wide voltage gain range by controlling the converter at frequencies both below and above the resonant frequency, primarily by varying the duty cycle. Although theoretical analysis indicates that a near-zero output voltage can be attained by reducing the duty cycle, this results in certain operating ranges where ZVS soft switching is not achievable. In these conditions, the turn-off current increases significantly, which leads to lower efficiency and greater EMI. Therefore, new methods for wide output regulation need to be explored. The 0.75× and 0.25× voltage gain modulation methods proposed in this paper offer a balance between wide voltage regulation and efficient operation. The proposed variable topology control strategy defines three discrete gain ratios (0.75, 0.5, and 0.25) at the resonant frequency. Along with the 1× fundamental ratio, this results in three distinct operating modes. Pulse Frequency Modulation (PFM) further enhances voltage regulation, and together these techniques enable a wide output voltage range.

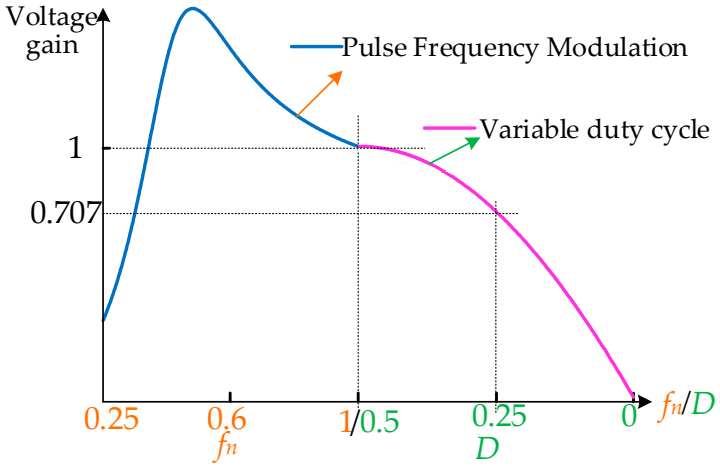



**Figure 5.** Normalized gain curves under conventional control methods with variable switching frequency or duty cycle.

## 3. Proposed Modulation and Control Method for Wide Gain

### *3.1. Proposed 0.75 Gain Operating Mode*

The modulation method proposed in Section 2 achieves a wide output voltage range through duty ratio variation. However, at small duty ratios, excessive resonant current spikes occur, leading to efficiency degradation. To achieve a wide gain range, the full-bridge T-type LLC converter employs variable-topology modulation, enabling multiple normalized gain points at the resonant frequency. The first part of this chapter presents the variable-topology modulation scheme that achieves a 0.75-times normalized gain, where the original reference normalization is unity gain. This introduces a 0.75-times voltage gain mode for the full-bridge T-type LLC converter operating at the resonant frequency. The 0.75-times gain mode consists of two frequency-controlled sub-modes (Mode 1 and Mode 2). Assuming that the voltages across $C_{dc1}$ and $C_{dc2}$ remain balanced at 0.5 $V_{in}$ with sufficient capacitance, Figure 6a,b show the equivalent circuit and operational waveforms for Mode 1, respectively.

When the converter operates in Mode 1 of the 0.75-times gain mode, $S_{a2}$ remains on, while $S_{a4}$, $S_{b2}$, and $S_{b3}$ stay off. $S_{a1}$ and $S_{a3}$ operate complementarily with a 50% duty cycle, and $S_{b1}$ and $S_{b4}$ operate complementarily with a 50% duty cycle, with a 180° phase

difference between $S_{b1}$ and $S_{a1}$. The converter exhibits the following operational phases within one cycle:

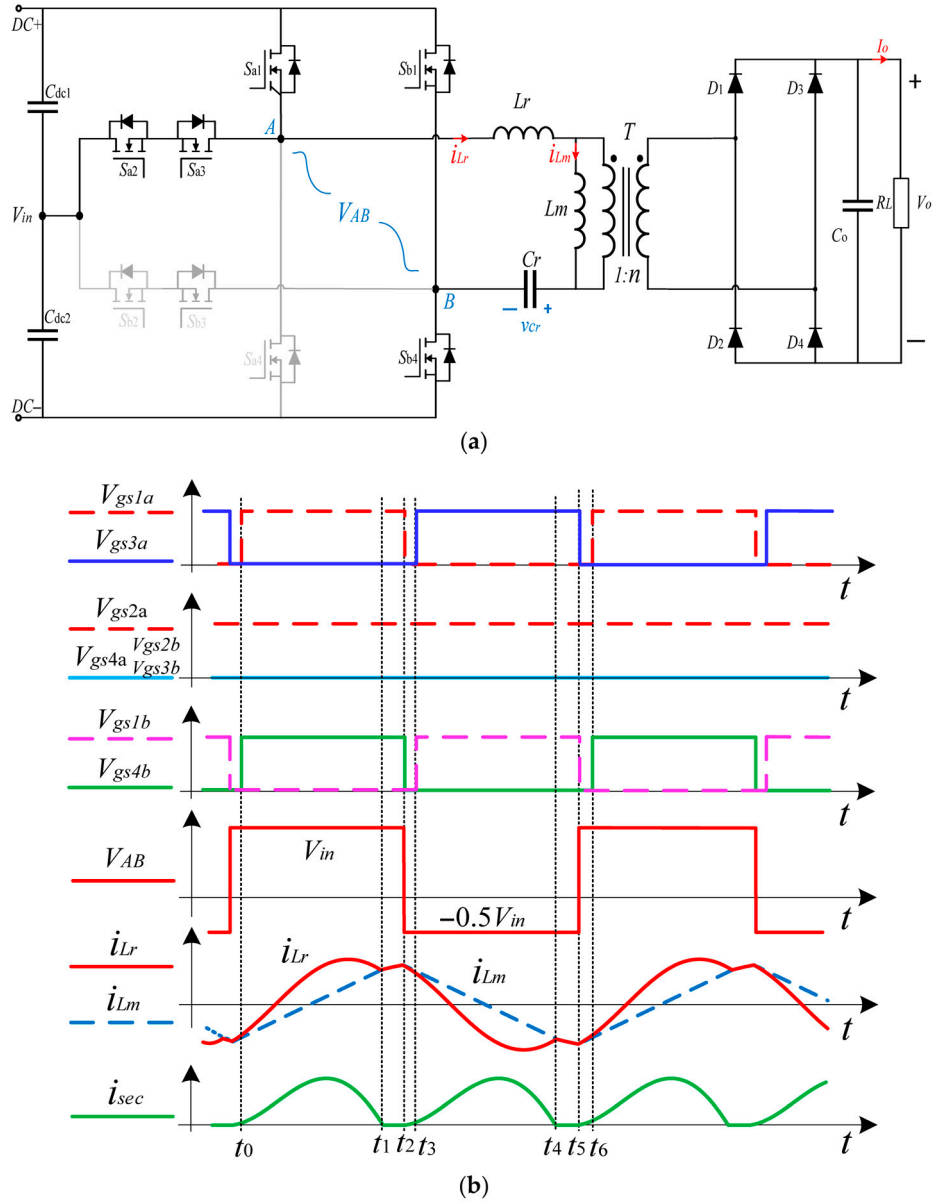



**Figure 6.** Circuit diagram and operating waveforms of 0.75 gain Mode I. (**a**) Equivalent circuit of Mode I; (**b**) waveforms of the Mode I circuit.

Phase [$t_0$–$t_1$]: During this phase, $S_{a1}$ and $S_{b4}$ conduct. The resonant tank input voltage $V_{AB}$ equals $V_{in}$, and the resonant inductor and capacitor resonate in series. The magnetizing inductance is clamped to $V_o/n$, causing its current to increase linearly.

Phase [$t_1$–$t_2$]: When the magnetizing current equals the resonant current, the primary and secondary sides of the transformer decouple, allowing the magnetizing inductance to resonate with the resonant inductor and capacitor.

Phase [$t_2$–$t_3$] (Dead Time): At $t_2$, $S_{a1}$ and $S_{b4}$ turn off. Since the resonant current remains positive, the circulating current flows through the body diodes of $S_{a3}$ and $S_{b1}$, changing the resonant tank input voltage to $-0.5\,V_{in}$. With the body diodes of $S_{a3}$ and $S_{b1}$ conducting, ZVS turn-on is achieved at $t_3$.

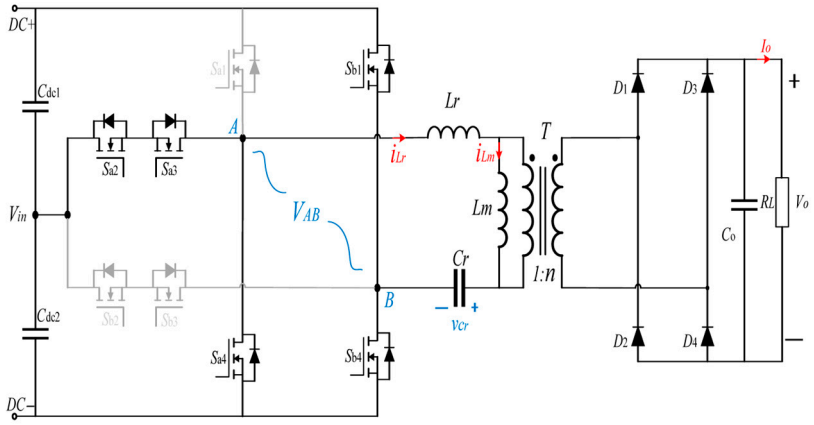
Phase [$t_3$–$t_4$]: With $S_{a3}$ and $S_{b1}$ conducting, the resonant tank input voltage is $-0.5\,V_{in}$. Since the resonant current is lower than the magnetizing current, the resonant inductor and

capacitor continue to resonate in series. The magnetizing inductance is clamped to $-V_o/n$, causing its current to decrease linearly.

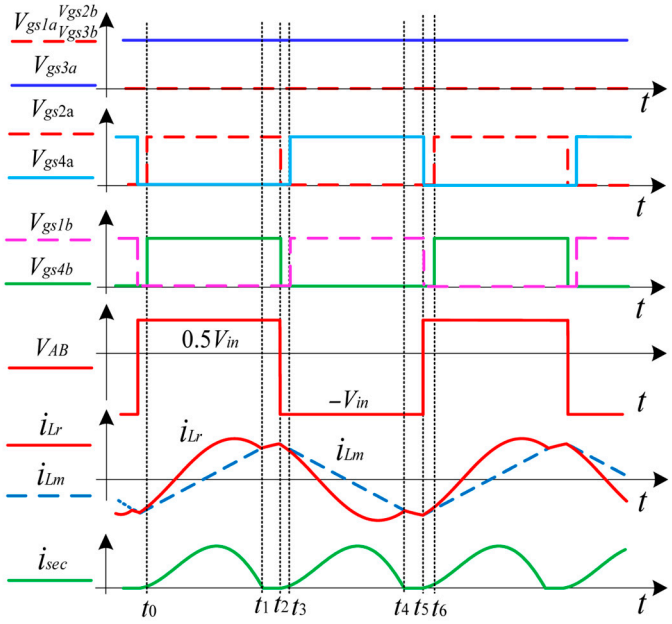
Phase [$t_4$–$t_5$]: When the resonant and magnetizing currents equalize, the transformer decouples again, allowing the magnetizing inductance to resonate with the resonant components.

Phase [$t_5$–$t_6$] (Dead Time): At $t_5$, $S_{a3}$ and $S_{b1}$ turn off. With negative resonant current, the current flows through the body diodes of $S_{a1}$ and $S_{b4}$, changing $V_{AB}$ to $V_{in}$. ZVS is achieved when $S_{a1}$ and $S_{b4}$ turn on after the dead time.

Mode 2 of the 0.75-times gain mode is symmetrical to Mode 1: $S_{a1}$, $S_{b2}$, and $S_{b3}$ remain off, while $S_{a3}$ stays on. $S_{a2}$ and $S_{a4}$ operate complementarily at a 50% duty cycle, as do $S_{b1}$ and $S_{b4}$. The corresponding waveforms and equivalent circuits are shown in Figures 6b and 7a, respectively. Given the high symmetry between the modes, where only $C_{dc2}$ replaces $C_{dc1}$ as the unilateral power source, the operational process of Mode 2 is omitted here.




(**a**)




(**b**)

**Figure 7.** Circuit diagram and operating waveforms of 0.75 gain Mode II. (**a**) Equivalent circuit of Mode II; (**b**) waveforms of the Mode II circuit.

Due to the presence of negative-voltage half-cycle intervals in 0.75-times gain Mode 1, the resonant network is powered solely by the upper input capacitor, $C_{dc1}$, during these periods. Similarly, in 0.75-times gain Mode 2, there is a duration where only the lower input capacitor, $C_{dc2}$, supplies power.

To maintain voltage balance between the input capacitors, the converter should alternate between both modes while operating in 0.75-times gain mode. This alternation prevents excessive voltage droop caused by prolonged operation of a single capacitor. Ideally, the converter operates in Mode 1 for a fixed duration (typically several dozen switching cycles in high-frequency operation), then switches to Mode 2 for an equal duration, repeating this sequence.

Thanks to the four-diode rectifier bridge on the secondary side, mode transitions have minimal impact on the output load. Consequently, the input voltage $V_{AB}$ of the resonant network can be approximated as a constant 0.75 $V_{in}$ during this process. In summary, the voltage-normalized gain formula for the full-bridge T-type LLC converter in 0.75-times gain mode is derived as follows:

$$G = \frac{0.75}{\sqrt{\left(1+\frac{1}{k}\left(1-\frac{1}{fn^2}\right)\right)^2+\left(Q^2\left(fn-\frac{1}{fn}\right)^2\right)}} \tag{2}$$

### *3.2. Proposed 0.25 Gain Operating Mode*

This section proposes a mode of operation for the full-bridge T-type LLC resonant converter that achieves a voltage gain of 0.25 at the resonant frequency, referred to as the 0.25-fold gain mode. This mode consists of two sub-modes, each controlled by frequency conversion. Assuming that the voltages across $C_{dc1}$ and $C_{dc2}$ are both 0.5 $V_{in}$ and that the capacitance is sufficiently large, the control method for Mode 1 of the 0.25-fold gain mode is as follows: switches $S_{a1}$, $S_{b1}$, $S_{b2}$, and $S_{b3}$ remain off, while switches $S_{a3}$ and $S_{b4}$ remain on, and switches $S_{a2}$ and $S_{a4}$ operate complementarily with a 50% duty cycle. The corresponding circuit waveforms and equivalent circuits are shown in Figures 8a and 8b, respectively.

Phase [$t_0$–$t_1$]: During this stage, $S_{a2}$ is conducting, and the resonant cavity input voltage ($V_{AB}$) is 0.5 $V_{in}$. Initially, the resonant inductor and resonant capacitor resonate in series, and the excitation inductance is clamped to $V_o/n$, with the current increasing linearly. Since $f_s < f_r$, the excitation inductance and resonant inductance resonate together towards the end of this stage when the excitation inductance equals the resonant inductance.

Phase [$t_1$–$t_2$]: The time interval between $t_1$ and $t_2$ is the dead time. At $t_1$, $S_{a2}$ turns off, and the resonant current becomes greater than zero. The resonant current loop is refreshed through the body diode of $S_{a4}$, and the resonant cavity input voltage becomes 0 V. After the dead time, at $t_2$, $S_{a4}$ can achieve ZVS turn-on.

Phase [$t_2$–$t_3$]: During this stage, $S_{a4}$ turns on. The resonant cavity input voltage remains at 0 V, and the resonant current is smaller than the excitation current. The resonant inductor and resonant capacitor continue to resonate in series. The excitation inductance is clamped to $-V_o/n$, causing the excitation current to decrease linearly. When the resonant current equals the excitation current, the transformer's primary and secondary sides are decoupled. At this point, the excitation inductance resonates with the resonant inductor and capacitor.

Phase [$t_3$–$t_4$] Stage: At $t_3$, $S_{a4}$ turns off, and the resonant current becomes negative. The resonant current is restored by the body diode of $S_{a2}$ and capacitor $C_{dc2}$, and $S_{a2}$ reverses conduction. The resonant cavity input voltage becomes $V_{in}$, after which $S_{a2}$ can achieve ZVS turn-on.

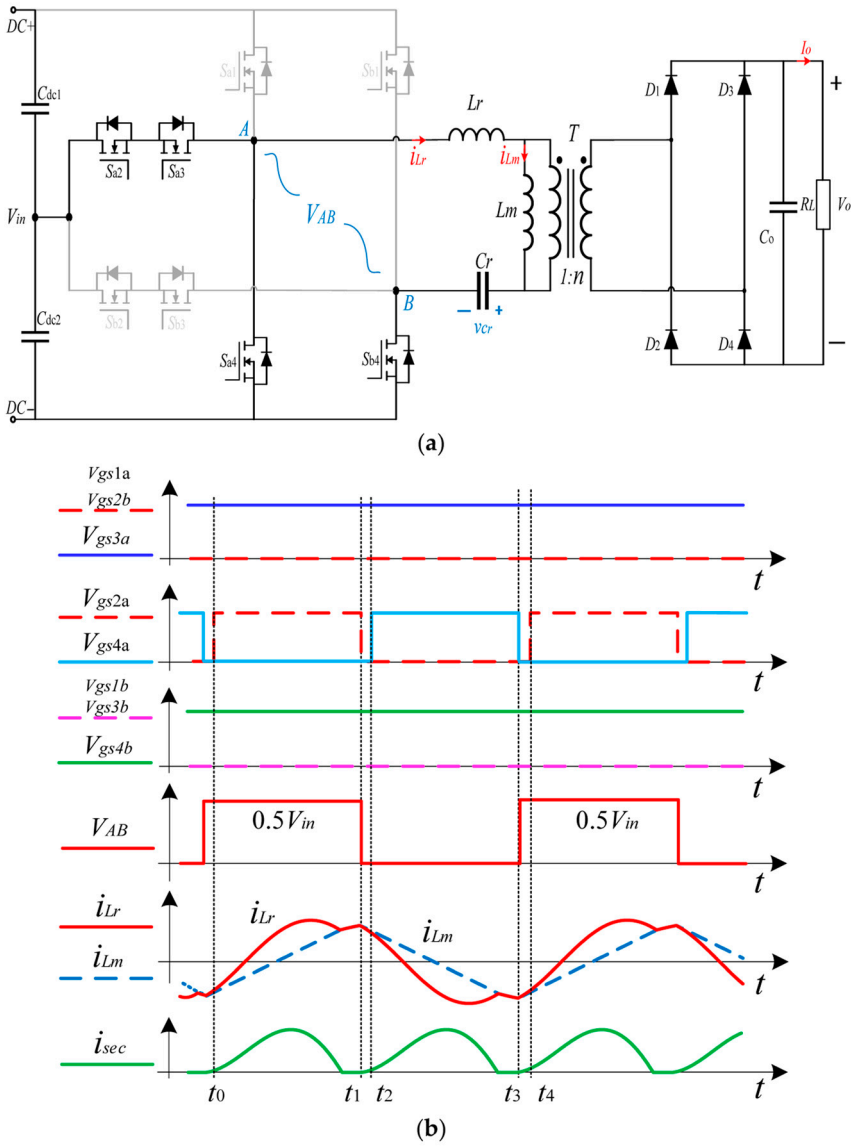



**Figure 8.** Circuit diagram and operating waveforms of 0.25 gain Mode I. (**a**) Equivalent circuit of Mode I; (**b**) waveforms of the Mode I circuit.

Mode II of the 0.25-times gain mode of the full-bridge T-type LLC converter is symmetrical to Mode I. When operating in Mode II, switches $S_{a2}$ and $S_{b1}$ remain continuously on, while switches $S_{a4}$, $S_{b2}$, $S_{b3}$, and $S_{b4}$ remain off. Switches $S_{a1}$ and $S_{a3}$ operate complementarily with a 50% duty cycle. The corresponding waveforms and equivalent circuits for this mode are shown in Figures 9a and 9b, respectively.

Using the fundamental harmonic approximation (FHA) method, it can be shown that the normalized DC voltage gain function of the full-bridge T-type LLC converter in both 0.25-times gain modes can be expressed by Equation (3). From Equation (3), it is evident that the voltage gain of the converter in both 0.25-times gain modes is 0.25 when the switching frequency equals the resonant frequency, representing only 0.25 times the voltage gain of the full-bridge mode with identical circuit parameters and switching frequency.

Since the initial voltages of $C_{dc1}$ and $C_{dc2}$ may not be balanced in practice, and since operating in a single mode would cause the capacitor voltage to drift, Mode 1 and Mode 2 of the 0.25-times gain mode should operate alternately. This alternation ensures that

the voltage across the dividing capacitors remains balanced within the desired range by controlling the duration of each mode.

$$G = \frac{0.25}{\sqrt{\left(1+\frac{1}{k}\left(1-\frac{1}{fn^2}\right)\right)^2 + \left(Q^2\left(fn-\frac{1}{fn}\right)^2\right)}} \tag{3}$$

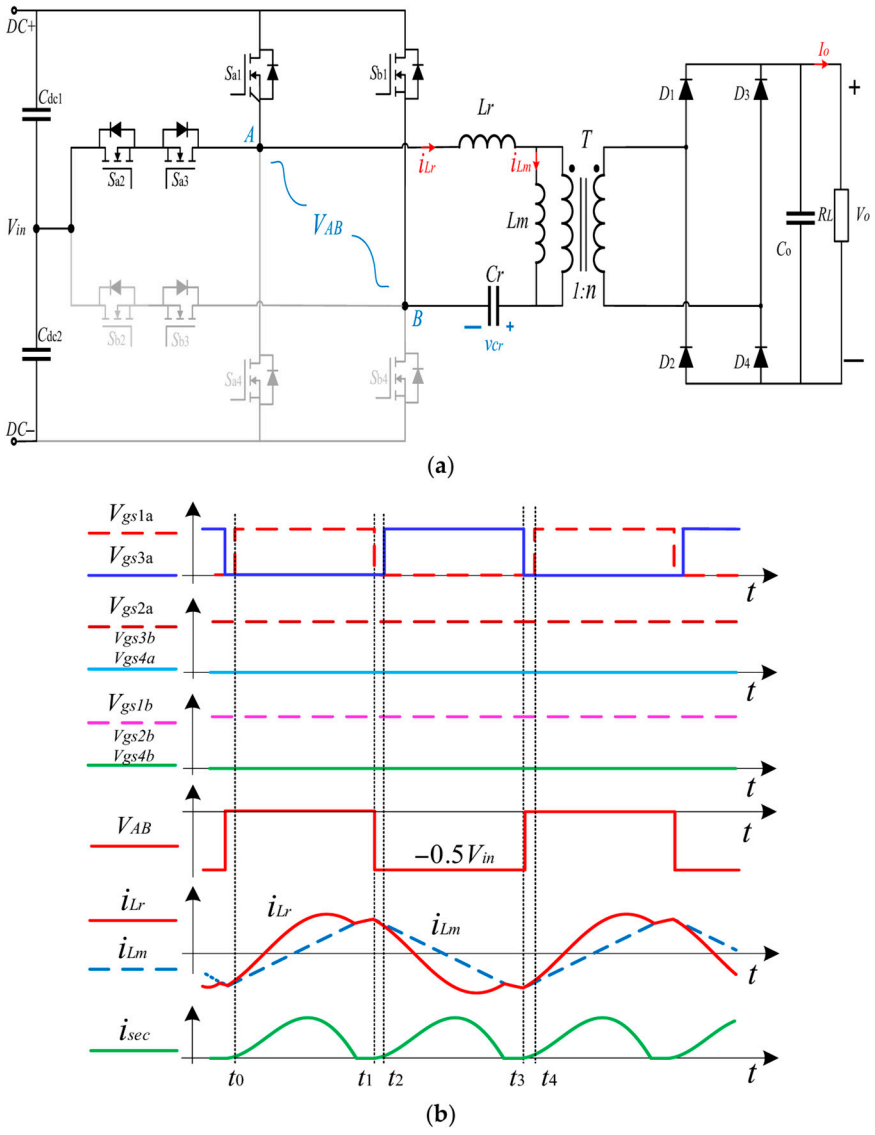



**Figure 9.** Circuit diagram and operating waveforms of 0.25 gain Mode II. (**a**) Equivalent circuit of Mode II; (**b**) waveforms of the Mode II circuit.

### *3.3. Conventional 1 and 0.5 Gain Operating Mode*

The conventional 1-times gain modulation method, introduced in Section 2, utilizes variable duty cycle and frequency modulation to achieve one times the normalized gain. This method is not repeated here. The full-bridge T-type three-level LLC converter, shown in Figure 10, operates in half-bridge mode, where $S_{a2}$ and $S_{a3}$ remain on, $S_{a1}$, $S_{a4}$, $S_{b2}$, and $S_{b3}$ remain off, and $S_{b1}$ and $S_{b4}$ operate with a 50% duty cycle.

The full-bridge T-type three-level LLC resonant converter operating in half-bridge mode undergoes the following stages during one cycle:

[$t_0$–$t_1$]: During this stage, $S_{b4}$ conducts, and the resonant cavity input voltage is 0.5 $V_{in}$.

[$t_1$–$t_2$]: At $t_1$, $S_{b4}$ is turned off. Since the resonant current is greater than zero, it forces the body diode of $S_{b1}$ to reverse conduction, renewing the current. After the current is renewed, the resonant cavity input voltage becomes $-0.5\ V_{in}$. The time interval from $t_1$ to $t_2$ is the dead time. At $t_2$, $S_{b1}$ turns on, and ZVS is achieved due to the reverse conduction during the turn-on.

[$t_2$–$t_4$]: The converter then enters the next half-cycle of operation, which is symmetric to the previous one (from $t_0$ to $t_2$). ZVS is also realized for $S_{b4}$ at $t_4$.

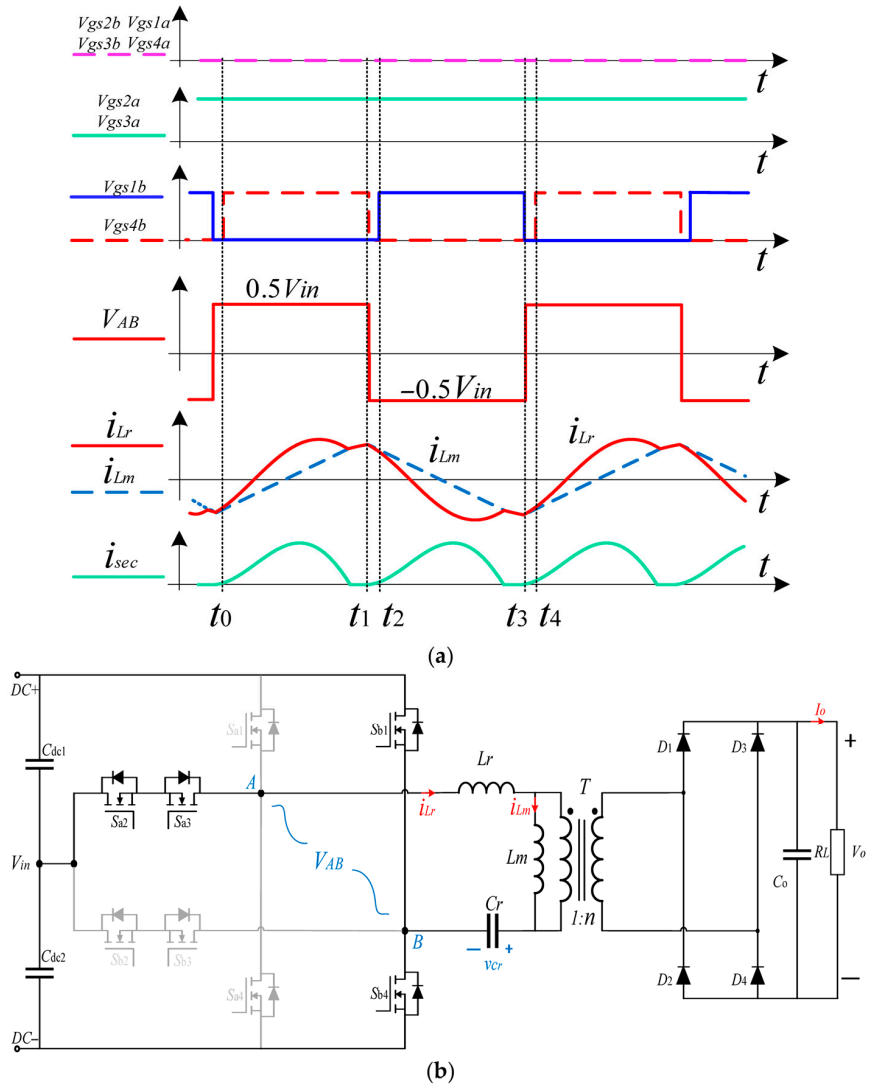



**Figure 10.** Waveforms and equivalent circuits at 0.5 gain half-bridge mode. (**a**) 0.5 gain operating waveform; (**b**) 0.5 gain operating equivalent plot.

Through the analysis of the 0.5-times gain mode, it can be seen that the alternate conduction of the upper and lower bridges not only reduces the voltage stress on the switching devices by half but also helps balance the input capacitors ($Vc_{dc1}$ = $Vc_{dc2}$), mitigating the effects of uneven voltage distribution. The normalized voltage gain in this modulation mode is as follows:

$$G = \frac{0.5}{\sqrt{\left(1+\frac{1}{k}\left(1-\frac{1}{fn^2}\right)\right)^2+\left(Q^2\left(fn-\frac{1}{fn}\right)^2\right)}} \tag{4}$$

### *3.4. Control Strategy of Full-Bridge T-Type Three-Level LLC Resonant Converter*

In summary, based on the gain function of the full-bridge T-type three-level LLC converter operating in different modes, the corresponding gain curves can be plotted, as shown in Figure 11. As seen in Figure 11, compared to the original operating modes, the proposed 0.75-times and 0.25-times gain modes enable the full-bridge T-type LLC converter to achieve an extended voltage gain range with minimal switching frequency variation, thereby enabling a wide output voltage range.

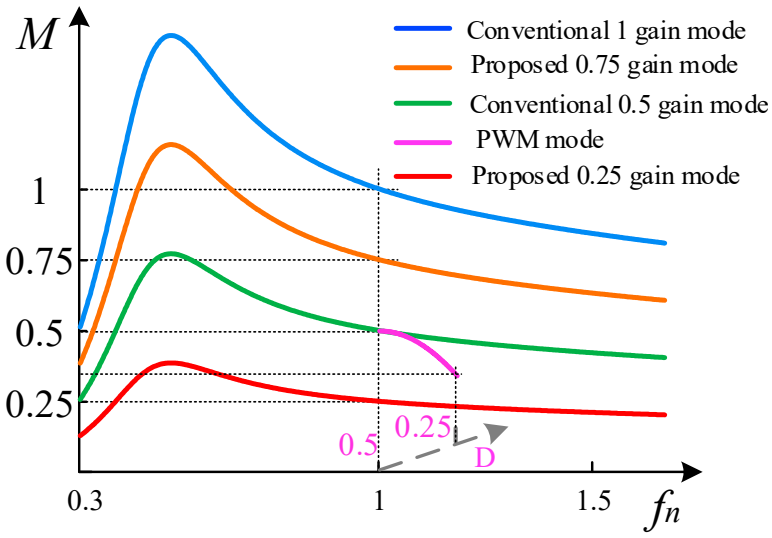



**Figure 11.** Normalized gain curves under the proposed method with variable circuit topology and switching frequency.

The full-bridge T-type three-level LLC resonant converter operates in four distinct modes, each of which is selected based on the gain range, as shown in Figure 12. The PI controller, $G_V$, adjusts the switching frequency according to the rated output voltage, $V_{ref}$. In this figure, $V_{ref}$ represents the reference output voltage, $V_O$ denotes the actual output voltage, and $V_{err}$ indicates the voltage error. Additionally, $G_{pre}$ refers to the predicted voltage gain, and $f_s$ represents the output frequency of the primary side inverter bridge section.

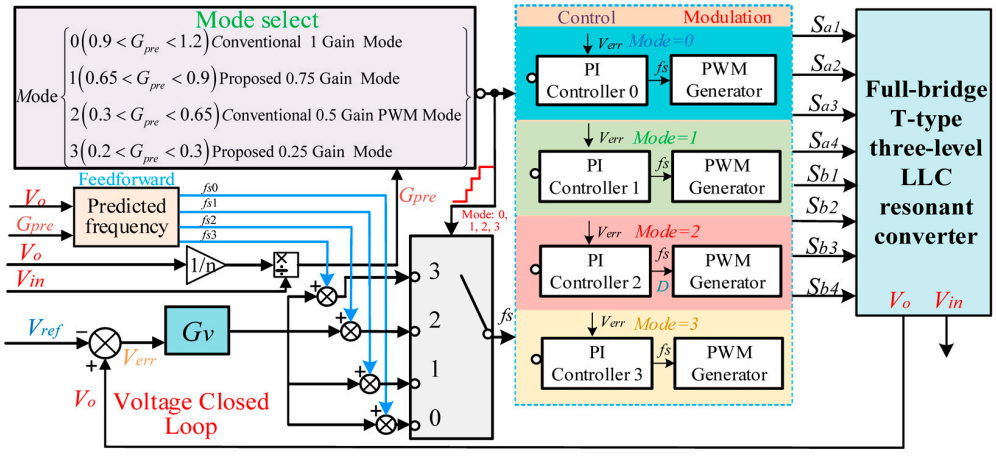



**Figure 12.** Proposed converter control block diagram based on quadruple normalized gain mode selection.

To enhance the accuracy of the converter's gain prediction, the mode prediction is incorporated into the mode selection process. Based on the output voltage, the required gain of the converter is determined, and the appropriate operation mode is selected accord-

ing to the voltage gain. The relationship between voltage gain and the mode of operation is described by a specific relational equation, as shown in the mode selection diagram in Figure 12. This approach enables the converter to achieve a wide output voltage range through mode selection and variable frequency control, resulting in a voltage gain of more than six times the normalized voltage.

## 4. Simulation and Experimental Results

### *4.1. Simulation of Different Modulation Modes for Full-Bridge T-Type Three-Level LLC Converter*

To verify the feasibility of the proposed modulation method to achieve the goal of wide voltage output, a complete simulation model of a full-bridge T-type three-level LLC resonant converter is constructed in this section based on the MATLAB/Simulink simulation platform. The main parameters of the simulation are shown in Table 1.

**Table 1.** Parameter table for simulation experiment of full-bridge T-type three-level LLC resonant converter.

| Component | Value | Component | Value |
|---|---|---|---|
| $V_{in}$ | 200 V | $L_r$ | 7.8 μH |
| $V_{out}$ | 100 V–400 V | $C_r$ | 900 nF |
| $f_r$ | 60 kHz | $L_m$ | 31.2 μH |
| $n$ | 2 | $R_{load}$ | 60 Ω |
| $C_{dc1}/C_{dc2}$ | 800 μF | | |

For the modulation method proposed in Section 3, simulation experiments were conducted to verify its effectiveness. As shown in Figure 13, with an input voltage of 200 V and a transformer turns ratio of 1:2 on both the primary and secondary sides, the system operates at a resonant frequency of 60 kHz. The output voltage was switched between 400 V and 100 V three times, as shown in the simulation waveforms. Figure 13 clearly demonstrates the feasibility of this modulation method, which meets the requirement for a four-fold output voltage ratio under resonant frequency conditions. Moreover, during the switching process, no overvoltage or overcurrent conditions occurred, preventing significant damage to the converter. The input filter capacitor voltage remained stable at approximately 100 V, with only a small deviation of about 0.5 V. This deviation can be attributed to the converter's balancing of capacitance charging and discharging during the switching between sub-modes.

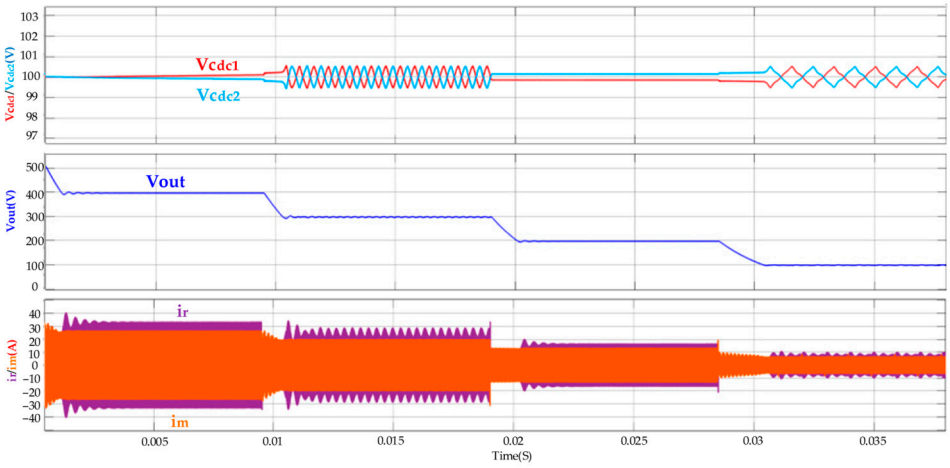



**Figure 13.** Dynamic simulation waveforms of output voltage change from 400 V to 100 V and waveforms of input capacitor voltage and resonant current and excitation current.

Figure 14 shows the simulated waveforms of the converter in the unity gain mode, with an input voltage of 200 V and operating at the resonant frequency. When a complementary drive signal is detected at unit gain and a dead time is applied, the reverse-connected T-type devices remain in the off state. At this point, the output voltage stabilizes around 400 V with a ripple of approximately 0.25%. Meanwhile, the secondary current follows a continuous half-sine waveform, enabling continuous energy transfer from the primary side to the secondary side.

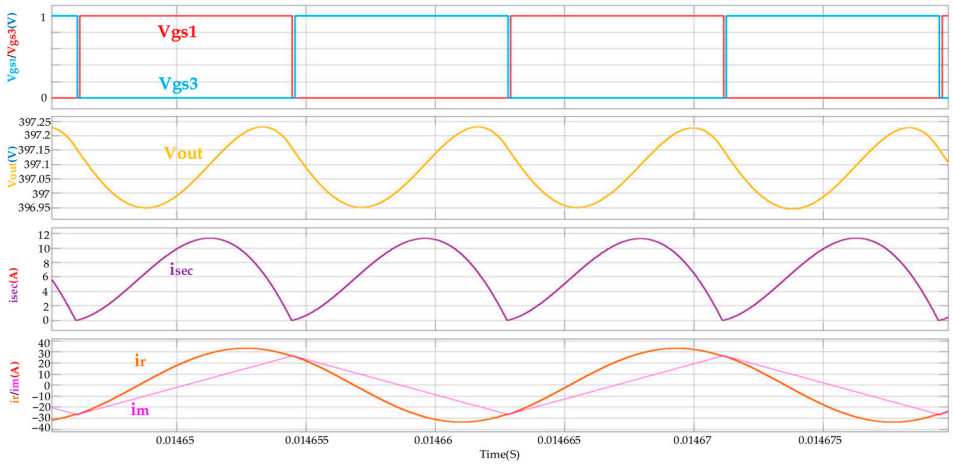



**Figure 14.** Steady-state waveforms in unity gain mode.

As shown in Figure 15, the simulated experimental waveform of the transition from sub-mode 1 to sub-mode 2 in 0.75-times gain mode is presented. It can be observed that the gate drive signal $V_{gs1}$ changes from a 50% duty cycle to a constant off state, while $V_{gs3}$ changes from a 50% duty cycle to a constant on state. With an input voltage of 200 V, the output voltage fluctuates around 300 V with a ripple rate not exceeding 1.67%. The switching process lasts 1 to 2 cycles, with minimal energy loss, no overcurrent in the resonant and excitation currents, and very little current jitter. This effectively achieves the transition between sub-modes while maintaining the voltage balance of the input capacitor. A 0.75-times modulation method is implemented at the resonant frequency, resulting in an output voltage that is 0.75 times the normalized gain.

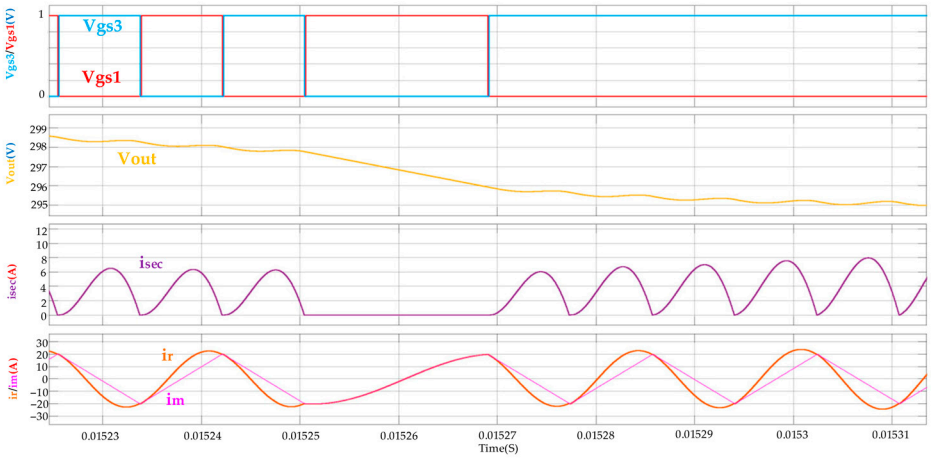



**Figure 15.** Dynamic transition waveform between two sub-circuit modes at a normalized voltage gain of G = 0.75.

As shown in Figure 16, the steady-state waveform of the bridge arm operation in 0.5× gain mode is presented. In this mode, the switching tubes $S_{a2}$ and $S_{a4}$ operate complemen-

tarily at the resonant frequency. The output voltage is half of the output voltage in the doubled gain mode, stabilizing around 200 V, with a ripple rate not exceeding 1.5%. The secondary-side current follows a continuous half-sinusoidal waveform, and energy is continuously transferred from the primary to the secondary side. Both the resonant current and excitation current remain within the permissible current range, ensuring that the converter achieves an output voltage half of the normalized gain at the resonant frequency.

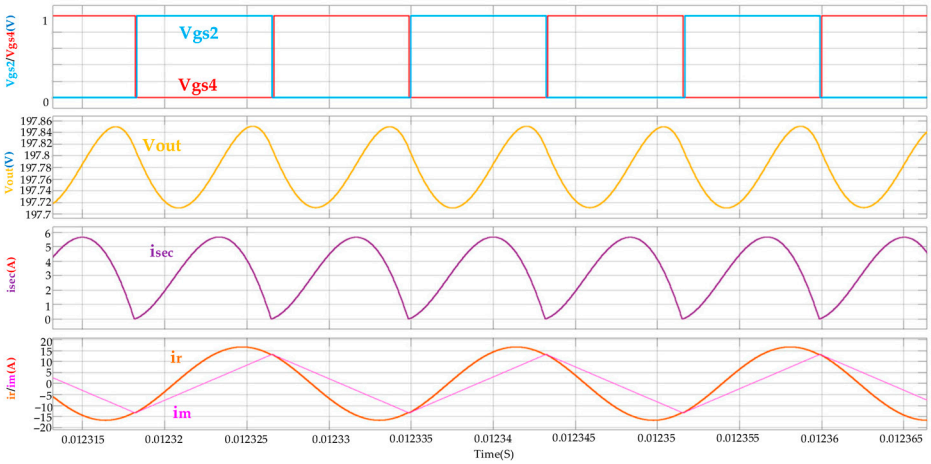



**Figure 16.** Steady-state waveform at a normalized voltage gain of G = 0.5.

As shown in Figure 17, the steady-state waveform of the switching process from sub-mode 2 to sub-mode 1 in the 0.25-times gain mode is presented. It can be observed that the gate drive signal $V_{gs1}$ changes from a 50% duty cycle to a constant off state, while $V_{gs3}$ changes from a 50% duty cycle to a constant on state. The input voltage is 200 V, and the output voltage fluctuates around 100 V, with a ripple rate not exceeding 3%. The switching process lasts for 1 to 2 cycles, with minimal energy loss, no overcurrent in the resonant and excitation currents, and minimal current jitter. This effectively enables switching between sub-modes while maintaining the voltage balance of the input capacitor. The resonant frequency is modulated by a factor of 0.25, resulting in an output voltage that is 0.25 times the normalized gain.

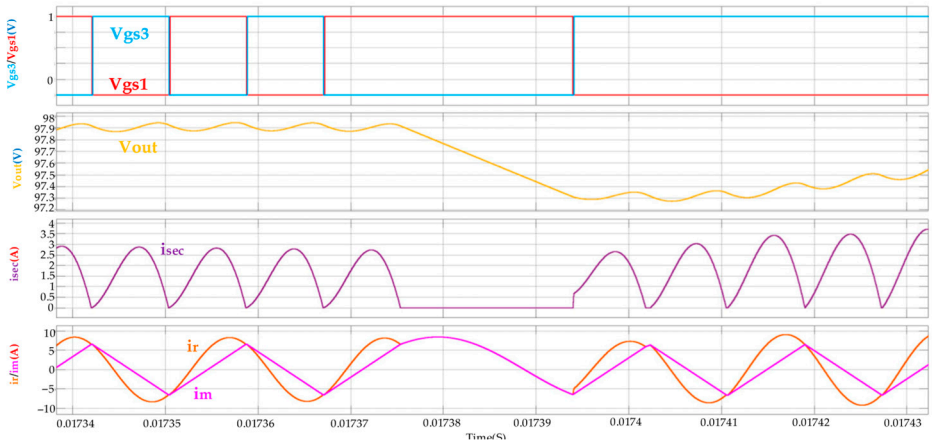



**Figure 17.** Dynamic transition waveforms between two sub-circuit modes at a normalized voltage gain of G = 0.25.

### *4.2. Experiments on Different Modulation Modes of Full-Bridge T-Type Three-Level LLC Converter*

To verify the feasibility of the output voltage in the proposed 0.75-fold and 0.25-fold gain modes and to achieve a wide output voltage range, a full-bridge T-type three-level

LLC resonant converter is constructed, as shown in Figure 18. The key parameters are as follows: Lr = 8.2 μH (including 0.4 μH transformer leakage inductance), *Cr* = 0.88 μF, *Lm* = 31.2 μH, *fr* = 58 kHz, and the transformer turns ratio *n* = 2. The MOSFET switching device is the STW70N60DM2 from STMicroelectronics. The rectifier diode is the VS-E5PX3006L-N3, and the controller used is the DSP F28377D.

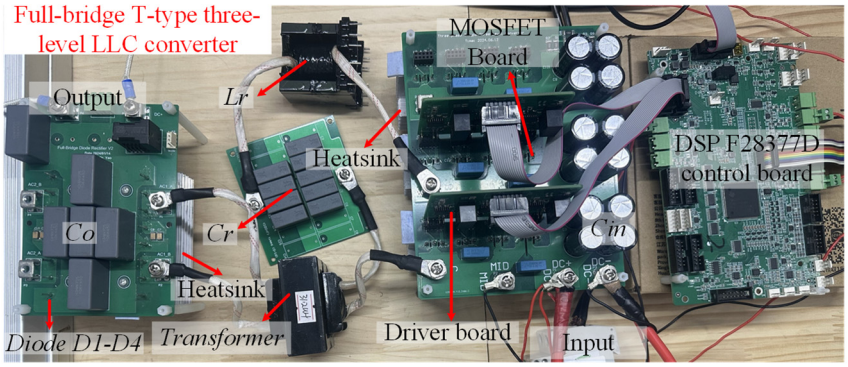



**Figure 18.** Full-bridge T-type three-level LLC resonant converter prototype.

As shown in Figures 19 and 20, the experimental waveforms are obtained under the traditional 1-times gain and 0.5-fold gain modes. The input voltage is a DC 200 V, and the switching frequency is 58 kHz. The output voltages are 400 V and 200 V, respectively, corresponding to the unity and 0.5-fold normalized voltage gain. The peak resonant currents are 26 A and 13 A, respectively, with the output load set to $R_{load}$ = 120 Ω. The experimental waveforms show that the output voltages are stable at 400 V and 200 V, with very small ripple. Additionally, the resonant inductor current and excitation inductor current align with the theoretical analysis and simulation results, confirming the validity and feasibility of the modulation scheme.

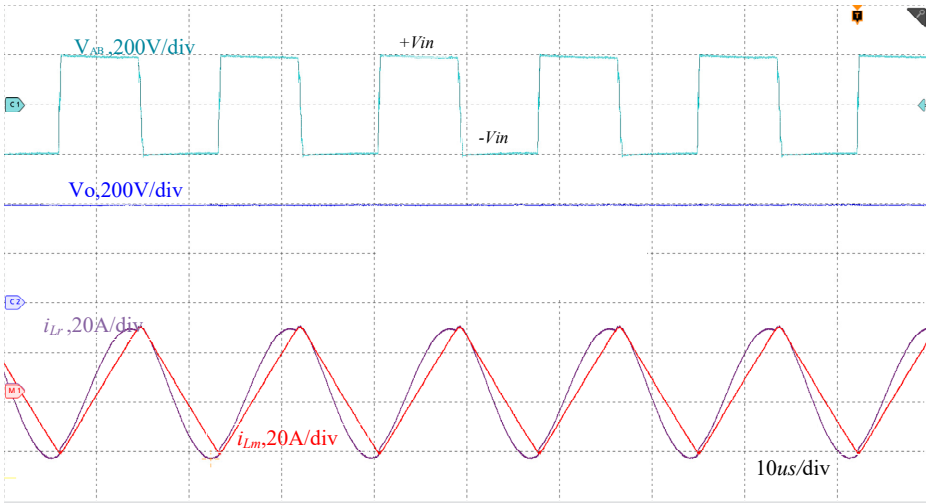



**Figure 19.** Experimental waveforms in conventional unity gain mode.

The dynamic experimental waveforms of the proposed 0.75-fold gain modulation mode, switching from sub-mode 2 to sub-mode 1, are shown in Figure 21. In sub-mode 2, the voltages of $V_{AB}$ are 0.5 times and −1 times the input voltage. After switching to sub-mode 1, the voltages of $V_{AB}$ become 1 and −0.5 times the input voltage. Both the theoretical analysis and simulation experiments validate the experimental waveforms, confirming their feasibility and correctness. During the switching process, there is no overcurrent in the resonant or excitation currents, which ensures the safety and reliability of the con-

verter's operation. The input voltage remains at DC 200 V, and the output voltage is 300 V with minimal ripple. The output load is set to $R_{load}$ = 120 Ω, and the switching frequency is 58 kHz, with a peak resonant current of 20.7 A.

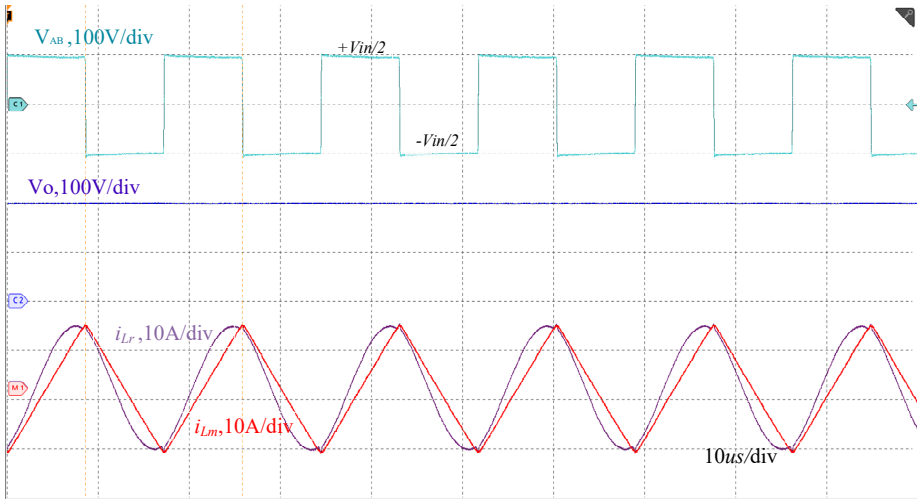



**Figure 20.** Experimental waveforms in conventional 0.5 gain mode.

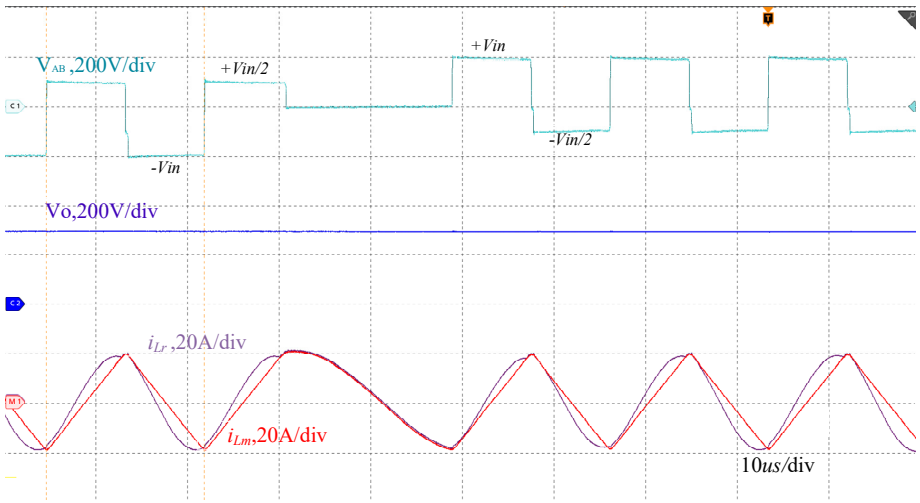



**Figure 21.** Dynamic experimental waveforms of the proposed 0.75-times gain mode switching from sub-mode 2 to sub-mode 1.

Figure 22 shows the steady-state experimental waveform after switching to sub-mode 2. In this sub-mode, the output voltage is 0.5 times and −1 times the input voltage, achieving 0.75 times the normalized gain of 300 V. The experimental waveforms align with the theoretical analysis and simulation results, proving that the modulation method is correct and feasible. This approach is conducive to achieving a wide voltage range output.

The dynamic experimental waveforms for the proposed 0.25-fold gain modulation mode, switching from sub-mode 2 to sub-mode 1, are shown in Figure 23. In sub-mode 2, the voltage of $V_{AB}$ is −0.5 times the input voltage. After switching to sub-mode 1, the voltage of $V_{AB}$ becomes 0.5 times the input voltage. Both theoretical analysis and simulation experiments validate the experimental waveforms, confirming their feasibility and correctness. During the switching process, neither the resonant current nor the excitation current exceeds the current limit, ensuring the safety and reliability of the converter's operation. The input voltage is maintained at 200 V DC, and the output voltage is 100 V with minimal ripple. The output load is set to $R_{load}$ = 120 Ω, the switching frequency is 58 kHz, and the peak resonant current is 9.2 A.

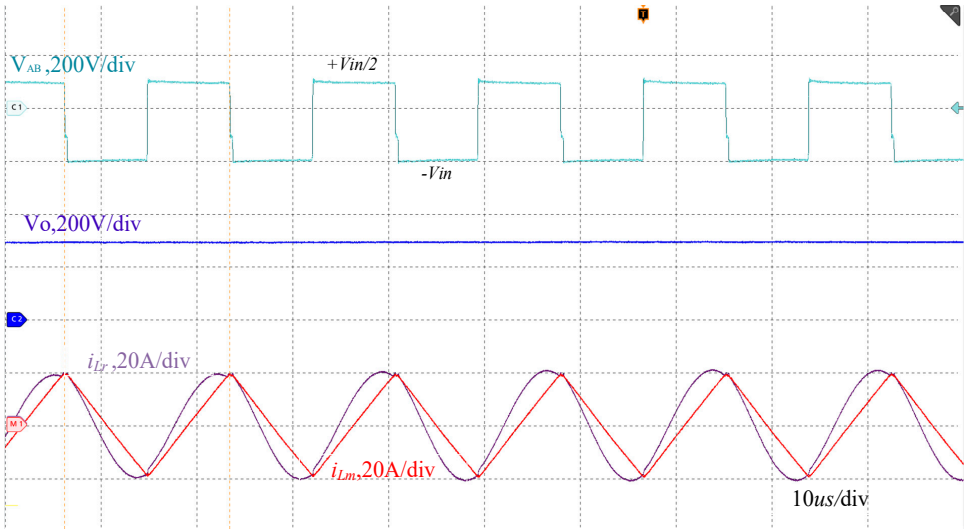



**Figure 22.** Proposed 0.75-times gain sub-mode 2 steady state experimental waveforms.

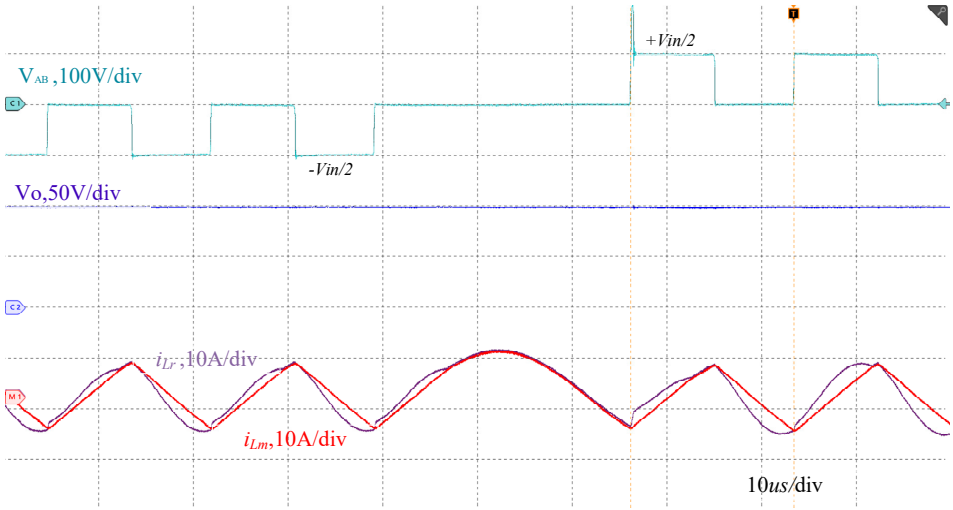



**Figure 23.** Dynamic experimental waveforms of the proposed 0.25-times gain mode switching from sub-mode 2 to sub-mode 1.

Figure 24 shows the steady-state experimental waveforms after switching to sub-mode 1. In this sub-mode, the output voltage is 0.5 times the input voltage, resulting in a normalized gain of 0.25 times 100 V. The experimental waveforms align with the theoretical analysis and simulation results, demonstrating the correctness and feasibility of the modulation method. This approach facilitates the realization of a wide voltage range output.

As shown in Figure 25, the heavy load waveform operates in 0.75-times gain mode with an input voltage of 100 V. Figure 26 presents the dynamic waveform of the output voltage, with the input voltage fixed at 100 V. Figure 26a shows the dynamic change of the voltage from 240 V to 180 V in 1-times gain mode, Figure 26b shows the dynamic change of the voltage from 180 V to 140 V in 0.75-times gain mode, Figure 26c shows the dynamic change of the voltage from 130 V to 90 V in 0.5-times gain mode, and Figure 26d shows the dynamic change of the voltage from 60 V to 50 V in 0.25-times gain mode. From the waveforms in these four sub-figures, it is evident that there is no over-voltage or over-current in the input voltage and resonant current during the voltage transition. This demonstrates that the converter can achieve a wide voltage range output by selecting different operating modes for voltage variation.

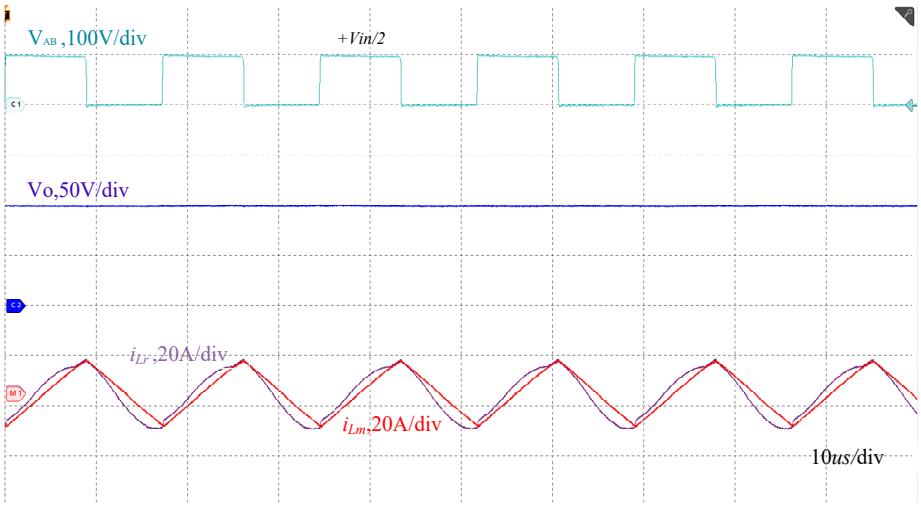



**Figure 24.** Proposed 0.25-times gain sub-mode 1 steady state experimental waveforms.

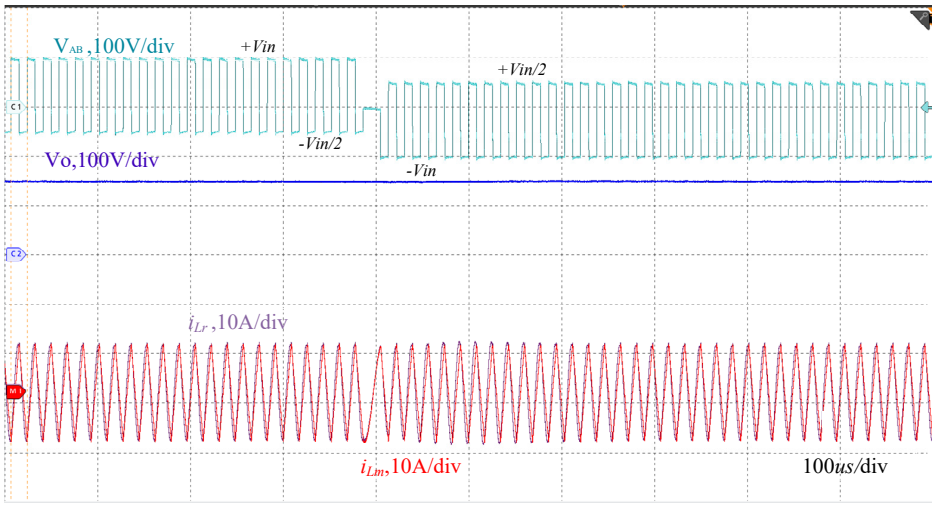



**Figure 25.** Heavy load waveforms in 0.75-times gain mode with 100 V input voltage.

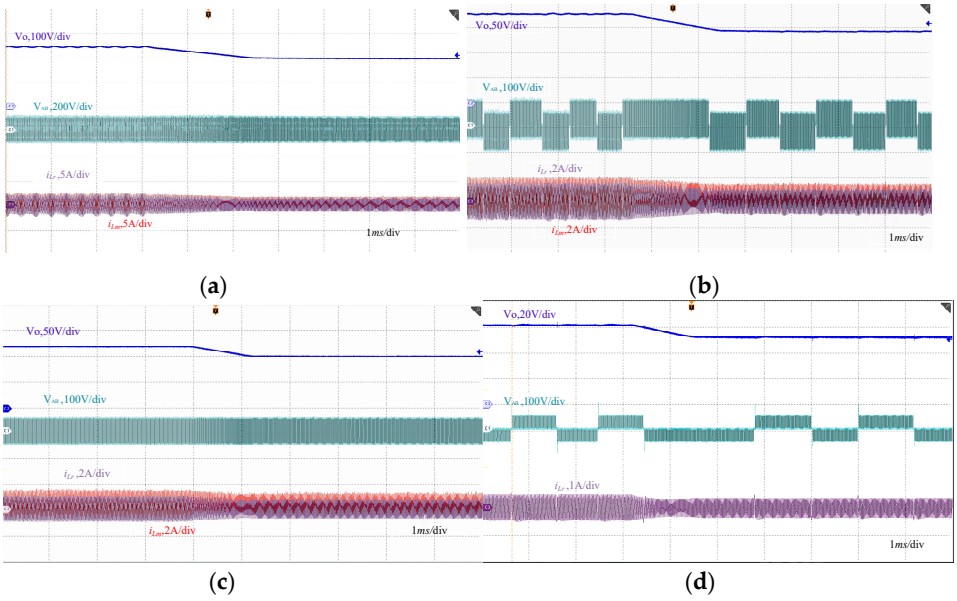



**Figure 26.** Output voltage dynamic response waveforms in different modes. (**a**) Conventional 1 gain mode; (**b**) 0.75 gain mode; (**c**) conventional 0.5 gain mode; (**d**) 0.25 gain mode.

The efficiency test results of the converter operating in the 0.75× gain mode are shown in Figure 27 with an input voltage of 200 V. At an output power of 1800 W and a switching frequency of 60 kHz, the converter achieves a conversion efficiency of 93.02%. These efficiency measurements for the proposed 0.75× gain modes at different output powers and frequencies verify the feasibility and effectiveness of the proposed method.

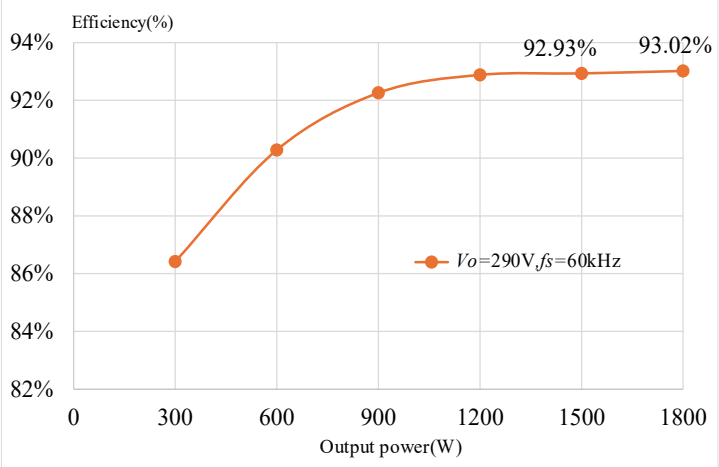



**Figure 27.** Efficiency at different output powers in 0.75× gain mode.

## 5. Conclusions

In this paper, a wide-output-voltage-range control method based on a full-bridge T-type three-level LLC resonant converter is proposed. The proposed 0.75-fold and 0.25-fold voltage gain modulation techniques effectively extend the output voltage range, addressing the challenges encountered by conventional LLC resonant converters in wide voltage applications. By combining the T-type three-level bridge arm with PWM modulation and employing a variable topology and frequency control strategy, the method successfully broadens the voltage gain range. Additionally, the PWM modulation method enhances the output voltage range by dynamically adjusting both the topology and frequency, effectively overcoming the limitations of traditional LLC converters. Simulation models and experimental prototypes developed in this study validate the effectiveness and feasibility of the proposed method. Experimental results demonstrate that the method achieves an input voltage of 100 V and an output voltage with a gain exceeding six times, reaching 40 V–240 V. This provides a reliable solution for applications requiring a wide output voltage range, such as new energy power generation systems and electric vehicle charging equipment. In the future, this converter can be applied to practical systems, such as electric vehicle charging or renewable energy interfaces.

**Author Contributions:** Conceptualization, K.Z. (Kangjia Zhang) and Z.Y.; Methodology, K.Z. (Kangjia Zhang) and Z.Y.; Software, M.L.; Validation, X.Y.; Formal analysis, K.Z. (Kun Zhao); Investigation, X.Y.; Resources, K.Z. (Kun Zhao); Data curation, K.Z. (Kangjia Zhang) and M.L.; Writing—original draft, K.Z. (Kangjia Zhang); Writing—review & editing, Z.Y. All authors have read and agreed to the published version of the manuscript.

**Funding:** This work was supported in part by Chengdu Guojia Electrical Engineering Company Ltd., under Grant NEEC-2022-B15.

**Data Availability Statement:** The original contributions presented in this study are included in the article. Further inquiries can be directed to the corresponding author.

**Conflicts of Interest:** The authors declare that this study received funding from Chengdu Guojia Electrical Engineering Company Ltd. The funder was not involved in the study design, collection, analysis, interpretation of data, the writing of this article, or the decision to submit it for publication.

## References

1. Fei, C.; Lee, F.C.; Li, Q. High-Efficiency High-Power-Density LLC Converter with an Integrated Planar Matrix Transformer for High-Output Current Applications. *IEEE Trans. Ind. Electron.* **2017**, *64*, 9072–9082. [CrossRef]
2. Kundu, U.; Yenduri, K.; Sensarma, P. Accurate ZVS Analysis for Magnetic Design and Efficiency Improvement of Full-Bridge LLC Resonant Converter. *IEEE Trans. Power Electron.* **2017**, *32*, 1703–1706. [CrossRef]
3. Yao, Z.; He, X.; Liu, M.; Liu, J.; Xiao, Z.; Tang, Y. Fixed Switching Frequency Control Using Trapezoidal Current Mode to Achieve ZVS in Three-Level DC-DC Converters. *IEEE Trans. Ind. Electron.* **2025**, *72*, 4175–4185. [CrossRef]
4. Wang, H.; Dusmez, S.; Khaligh, A. Design and Analysis of a Full-Bridge LLC-Based PEV Charger Optimized for Wide Battery Voltage Range. *IEEE Trans. Veh. Technol.* **2014**, *63*, 1603–1613. [CrossRef]
5. Deng, J.; Li, S.; Hu, S.; Mi, C.C.; Ma, R. Design Methodology of LLC Resonant Converters for Electric Vehicle Battery Chargers. *IEEE Trans. Veh. Technol.* **2014**, *63*, 1581–1592. [CrossRef]
6. Mustafa, A.; Mekhilef, S. Dual Phase LLC Resonant Converter with Variable Frequency Zero Circulating Current Phase-Shift Modulation for Wide Input Voltage Range Applications. *IEEE Trans. Power Electron.* **2021**, *36*, 2793–2807. [CrossRef]
7. Lin, J.; Yueh, H.; Lin, Y.; Liu, P. Variable-Frequency and Phase-Shift with Synchronous Rectification Advance On-Time Hybrid Control of LLC Resonant Converter for Electric Vehicles Charger. *IEEE J. Emerg. Sel. Top. Ind. Electron.* **2023**, *4*, 348–356. [CrossRef]
8. Wei, Y.; Luo, Q.; Mantooth, A. Overview of Modulation Strategies for LLC Resonant Converter. *IEEE Trans. Power Electron.* **2020**, *35*, 10423–10443. [CrossRef]
9. Zhang, J.; Cai, Z. Hybrid Control Switching Technology for LLC Resonant Converter. *Energies* **2024**, *17*, 6250. [CrossRef]
10. Jiang, H.; Yue, X. Phase-Shifting Adaptive LLC Resonant Converter with Reduced Turn-Off Loss in Wide Voltage Application. *Energies* **2024**, *17*, 1555. [CrossRef]
11. Dou, Y.; Ai, S.; Cheng, S.; Fang, S. Hybrid Control and Optimal Parameters Design for Wide Input Range Series Half Bridge Three Level LLC Resonant Converter in UUV Power Supply System. *IEEE Trans. Transp. Electrif.* **2025**, *1*, 1. [CrossRef]
12. Yue, Y.; Liu, Y.; Zhang, J.; Zhao, H.; Yang, J. Hybrid Control Method of Full-Bridge LLC Resonant Converter Based on Electric Vehicle. *IEEE Access* **2024**, *12*, 51859–51868. [CrossRef]
13. Luo, G.; Yao, Z.; Jiang, L.; Xiao, Z.; Chen, W.; Tang, Y. Current Balancing Control Method with Reduced Number of Current Sensors for Interleaved LLC Converters. *IEEE J. Emerg. Sel. Top. Power Electron.* **2024**, *12*, 2604–2613. [CrossRef]
14. Gao, L.; Liu, K.; Chen, Y.; Luan, H.; Zhou, S.; Cai, H. Variable-Gain LLC Converter with Series–Parallel Hybrid Switch-Controlled Capacitor Network. *IEEE Trans. Power Electron.* **2025**, *40*, 3885–3898. [CrossRef]
15. Hou, Z.; Jiao, D.; Lai, J.-S. An Ultrawide Range Pulse Width Modulated LLC Converter with Voltage Multiplier Rectifiers. *IEEE Trans. Power Electron.* **2025**, *40*, 6216–6229. [CrossRef]
16. Ning, G.; Du, L.; Xu, G.; Sun, Y.; Liu, Y.; Han, H. Dual-Mode LLC Converter with Wide Voltage Gain in Narrow Switching Frequency Range. *IEEE Trans. Power Electron.* **2024**, *39*, 12058–12064. [CrossRef]
17. Wei, Y.; Luo, Q.; Mantooth, A. Comprehensive Analysis and Design of LLC Resonant Converter with Magnetic Control. *CPSS Trans. Power Electron. Appl.* **2019**, *4*, 265–275. [CrossRef]
18. Zhu, L.; Sheng, Z.; Peng, F.; Yang, L. Control Strategy of Half-Bridge Three-Level LLC Resonant Converters with Wide Output Voltage Range. *IEEE Trans. Plasma Sci.* **2022**, *50*, 4381–4386. [CrossRef]
19. Yao, Z.; Liu, M.; Li, Y.; Xiao, Z.; Jiang, Y.; Zhang, L. Generalized Trapezoidal Current Mode-Based Zero-Voltage Switching for Multilevel DC-DC Converters. *IEEE Trans. Power Electron.* **2025**, *40*, 8956–8961. [CrossRef]
20. Qin, J.; He, Z.; Weng, Z.; Guan, R.; Li, Z.; Li, Z. Serial Hybrid-Clamped Three-Level Half-Bridge LLC Resonant Converter with Wide Input Voltage Range. *IEEE Trans. Ind. Electron.* **2024**, *71*, 13991–14001. [CrossRef]
21. Chen, J.; Wang, Z.; Lan, Y.; Zeng, L.; Xiong, X.; Wang, W. A Novel Five-level LLC Resonant Converter and Its Modulation Strategy. In Proceedings of the 2024 IEEE 8th Conference on Energy Internet and Energy System Integration (EI2), Shenyang, China, 29 November–2 December 2024; pp. 3714–3719. [CrossRef]
22. Jiang, T.; Zhang, J.; Wu, X.; Sheng, K.; Wang, Y. A Bidirectional Three-Level LLC Resonant Converter with PWAM Control. *IEEE Trans. Power Electron.* **2016**, *31*, 2213–2225. [CrossRef]
23. Yao, Z.; He, X.; Lan, H.; Yang, H.; Xiao, Z.; Deng, F. A Trapezoidal Current Mode to Reduce Peak Current in Near-CRM for Three-Level DC–DC Converter. *IEEE Trans. Power Electron.* **2024**, *39*, 9446–9456. [CrossRef]
24. Jin, K.; Ruan, X. Hybrid Full-Bridge Three-Level LLC Resonant Converter—A Novel DC–DC Converter Suitable for Fuel-Cell Power System. *IEEE Trans. Ind. Electron.* **2006**, *53*, 1492–1503. [CrossRef]

25. Rashwan, A.; Sayed, M.A.; Mobarak, Y.A.; Shabib, G.; Senjyu, T. Predictive Controller Based on Switching State Grouping for a Modular Multilevel Converter with Reduced Computational Time. *IEEE Trans. Power Deliv.* **2017**, *32*, 2189–2198. [CrossRef]
26. Jia, P.; Liu, M. A Wide Range LLC Resonant Converter Realized by an Adjustable Turns Ratio Transformer. *IEEE Trans. Power Electron.* **2025**, *40*, 10396–10401. [CrossRef]
27. Li, G.; Yang, D.; Zhou, B.; Zhang, H. A Topology-Reconfigurable LLC Resonant Converter for Wide Output Range Applications. *IEEE Trans. Veh. Technol.* **2022**, *71*, 10389–10399. [CrossRef]
28. Zuo, Y.; Shen, X.; Du, B.; Sui, Q.; Geboers, T.; Martinez, W. Reconfigurable LLC Resonant Converter for Wide Voltage Range and Reduced Voltage Stress in DC-Connected EV Charging Stations. In Proceedings of the 2025 IEEE Applied Power Electronics Conference and Exposition (APEC), Atlanta, GA, USA, 16–20 March 2025; pp. 436–441. [CrossRef]
29. Xue, Y.; Yang, G. A Wide-Output-Range DC-DC Converter and Minimum Loss Collaborative Control Strategy. *Energies* **2024**, *17*, 499. [CrossRef]
30. Alaql, F.; Alfraidi, W.; Alhatlani, A.; Al-Shamma'a, A.A.; Hussein Farh, H.M.; Allehyani, A. A Detailed Analysis and Gain Derivation of Reconfigurable Voltage Rectifier-Based LLC Converter. *Electronics* **2024**, *13*, 3788. [CrossRef]
31. Hao, Z.; Yang, Y.; Li, H. Design of "十" Low Turn Ratio Planar Transformer in High Transformation Ratio LLC Resonant Converter. In Proceedings of the 2024 IEEE 10th International Power Electronics and Motion Control Conference (IPEMC2024-ECCE Asia), Chengdu, China, 17–20 May 2024; pp. 3781–3786. [CrossRef]
32. Khodabakhsh, J.; Moschopoulos, G. A T-Type DC-DC Converter with Reduced Middle-Leg Switch Current Stress and Improved Light-Load Efficiency. *IEEE Open J. Power Electron.* **2020**, *1*, 238–249. [CrossRef]
33. Sun, X.; Li, X.; Shen, Y.; Wang, B.; Guo, X. Dual-Bridge LLC Resonant Converter with Fixed-Frequency PWM Control for Wide Input Applications. *IEEE Trans. Power Electron.* **2017**, *32*, 69–80. [CrossRef]
34. Yao, Z.; Jiang, L.; Sun, T.; Xiao, Z.; Chen, W.; Tang, Y. Smooth Optimal Trajectory and Voltage Balancing Control for T-Type Three-Level LLC Resonant Converter in Alternating Mode. *IEEE Trans. Power Electron.* **2025**, *40*, 9278–9288. [CrossRef]
35. Jiang, L.; Yao, Z.; Luo, G.; Yang, B.; Chen, W. Design and Control Method of T-Type Three-Level LLC Converter for Wide Input Voltage Application. In Proceedings of the 2024 IEEE 10th International Power Electronics and Motion Control Conference (IPEMC2024-ECCE Asia), Chengdu, China, 17–20 May 2024; pp. 2122–2127. [CrossRef]
36. Ma, W.; Li, H.; Yin, S.; Pang, X.; Chu, D. Design of Hybrid SiC/Si Based T-Type Three-Level LLC Resonant Converter with Wide-Input Range and Low Conduction Loss for Automotive Auxiliary Power Module. *IET Power Electron.* **2023**, *16*, 209–226. [CrossRef]
37. Queiroz, S.S.; Costa, L.F. Optimal Design of a LLC Resonant DC-DC Converter Based on the Stacked Half-Bridge Concept for Solid-State Transformer. *IEEE Trans. Power Electron.* **2025**. [CrossRef]
38. Qin, J.; Li, Z.; He, Z.; Weng, Z.; Guan, R.; Li, Z. Thermal Balance Modulation of Switching Devices for Hybrid-Clamped Three-Level Full-Bridge LLC Resonant Converter. *IEEE Trans. Power Electron.* **2024**, *39*, 5487–5497. [CrossRef]
39. Yao, Z.; He, X.; Xiao, Z.; He, Z.; Jiang, Y.; Tang, Y. Full-Range ZVS Control Method Based on Near-CRM for T-Type Three-Level Inverter. In Proceedings of the 2023 IEEE Energy Conversion Congress and Exposition (ECCE), Nashville, TN, USA, 29 October–2 November 2023; pp. 2987–2992. [CrossRef]
40. Shi, Y.; Wang, L.; Xie, R.; Shi, Y.; Li, H. A 60-kW 3-kW/kg Five-Level T-Type SiC PV Inverter with 99.2% Peak Efficiency. *IEEE Trans. Ind. Electron.* **2017**, *64*, 9144–9154. [CrossRef]
41. Wei, Y.; Zhang, S.; Liu, J.; Mantooth, H.A. Hybrid PFM and PWM Modulation Strategy for Stacked Structure LLC Resonant Converter with Wide Input Voltage Range Application. *IEEE Trans. Ind. Appl.* **2024**, *60*, 4038–4053. [CrossRef]
42. Kirshenboim, O.; Peretz, M.M. Combined Multilevel and Two-Phase Interleaved LLC Converter with Enhanced Power Processing Characteristics and Natural Current Sharing. *IEEE Trans. Power Electron.* **2018**, *33*, 5613–5620. [CrossRef]


**Disclaimer/Publisher's Note:** The statements, opinions and data contained in all publications are solely those of the individual author(s) and contributor(s) and not of MDPI and/or the editor(s). MDPI and/or the editor(s) disclaim responsibility for any injury to people or property resulting from any ideas, methods, instructions or products referred to in the content.